Target Surface pBRDF Model Optimization and Polarization Characteristics Analysis

Qiang Fu, Xuanwei Liu, Liya Wang, Juntong Zhan, Su Zhang, and Jin Duan

***Abstract*—In this paper, the scattering characteristics of polarized light are studied based on the microsurface element theory, and the Polarization Bi-directional Reflection Distribution Function (pBRDF) model applicable to rough surfaces is established according to the three-component model, and the expression of polarization of reflected light from the target surface is derived based on the model, and the accuracy of the model is verified by comparing the model with the conventional model. The modeling is also carried out from the scattering perspective, and the relationship between different artificial target particle diameters and polarization characteristics is analyzed. The results show that the Degree Of Polarization (DOP) is strongly related to the detection zenith angle. The DOP of the target is largest in the direction of the mirror reflection of the source. The polarization characteristics of different materials are different, and the relative error of the established model is significantly smaller than that of the conventional model. And the scattering model can make preliminary classification of different man-made targets according to different particle diameters, which can provide theoretical support for the analysis of the polarization characteristics of the target surface.**

***Index Terms*—Azimuth angle, polarization detection, scattering model, three-component, zenith angle.**

I. Introduction

WHEN a light beam is refracted or reflected on the surface of an optical medium, the polarization state of the beam will change due to the medium's own properties, which are influenced by various factors such as the roughness of the object surface, the refractive index of the medium, the observation angle, and the medium's own properties [1], [2], [3], [4], [5].

The target can be identified by obtaining the polarization information of the target. Polarization detection technology can achieve the characterization of the target by obtaining the polarization information of the target, analyzing the difference of the polarization characteristics of the target, and improving the contrast of the polarization between the targets, which can better identify and distinguish the targets [6], [7], [8].

The Bidirectional Reflectance Distribution Function (BRDF) represents the reflectance properties of an object surface at any observation angle for different light incidence angles, and is a deterministic function to describe the light reflection properties of an object surface. Since the 1980s, BRDF has been studied worldwide, and breakthroughs have been achieved [9], [10], [11]. With the accumulation of data and deeper understanding, researchers investigated the mechanism of the generation of the polarization properties of reflected light [12], [13]. Since 2000, researchers began to extend the common BRDF model in fully polarized form, and in the same year, Priest at the U.S. Naval Laboratory successfully polarized the Torrance-Sparrow model (T-S model) by combining the classical T-S model with the Mueller matrix, starting from a small surface element. Two years later, he conducted a polarization comparison of two samples based on this theory, and after comparing the data obtained from experimental measurements with the model, he concluded that high absorption has a greater effect on the polarization of rough object surfaces than high reflection.

Most of the above methods for target identification using polarization information are only limited to the analysis of polarization images, and do not fully utilize the unique polarization properties generated by light irradiation on the target surface. Therefore, in this paper, the polarization properties of the target surface are modeled. Fresnel's formula is introduced to describe the distribution of energy in reflected and refracted light, and the pBRDF model based on the microfacet metamodel is derived by considering the polarization effect existing when reflection occurs, establishing the conversion relationship of polarization states during light reflection, and improving on it to derive the three-component-based pBRDF model. Simulation analysis is performed according to the proposed model, and then the simulation data of the proposed model and the base model are compared with the measured data for analysisIt. Is demonstrated that the optimized pBRDF model can provide theoretical support for analyzing the polarization characteristics of the target surface.

II. Principle of Polarization Reflection Characteristics and Modeling

Bi-directional Reflection Distribution Function (BRDF) is the ratio of the incident light incident to the surface of the object after reflection of the outgoing radiant luminance to the radiant illuminance of the incident light [14], and its expression is.

$$f_{\mathrm{r}}(\theta_{\mathrm{i}}, \varphi_{\mathrm{i}}, \theta_{\mathrm{r}}, \varphi_{\mathrm{r}}, \lambda) = \frac{dL_{\mathrm{r}}(\theta_r, \varphi_{\mathrm{r}}, \lambda)}{dE_{\mathrm{i}}(\theta_{\mathrm{i}}, \varphi_{\mathrm{i}}, \lambda)} \tag{1}$$

Where λ is the wavelength; dL_{r} is the outgoing irradiance of the target, defined as the irradiance flux per unit area and per unit stereo angle, in W/(m2sr); $dE_{\mathrm{i}}$is the irradiance of the incident

Manuscript received 28 November 2022; revised 23 January 2023; accepted 9 February 2023. Date of publication 13 February 2023; date of current version 24 February 2023. *(Corresponding author: Qiang Fu.)*

The authors are with the College of Opto-Electronic Engineering, Changchun University of Science and Technology, Changchun 130012, China (e-mail: cust_fuqiang@163.com; 1731902794@qq.com; 627602950@qq.com; zhanjuntong@cust.edu.cn; susiezhang21@126.com; duanjin@vip.sina.com).

Digital Object Identifier 10.1109/JPHOT.2023.3244505

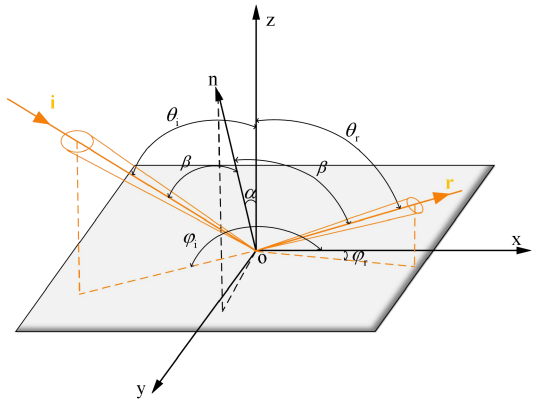

Fig. 1. Geometric relationship diagram of microplane elements.

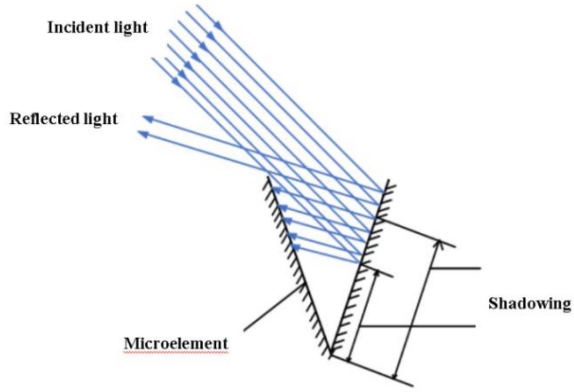

Fig. 2. Schematic diagram of simultaneous shading and masking effects.

light on the target surface, defined as the irradiance flux per unit area along the radiation direction, in W/m2; f_{r} is their ratio, in sr-1.

The BRDF represents the reflection characteristics of the object surface at any observation angle for different light incident angles, and is a deterministic function to describe the light reflection characteristics of the object surface. The microsurface element model in this paper adopts the Gaussian distribution as the probability distribution function of the normal distribution of microsurface elements on the rough object surface [15], and the expression is.

$$p(\alpha) = \frac{1}{2\pi\sigma^2\cos^3(\alpha)} \exp\left[\frac{-\tan^2(\alpha)}{2\sigma^2}\right] \tag{2}$$

Where, α is the angle between the micro surface metric normal and the macro normal of the rough surface, and $\sigma$is the arithmetic mean difference of the target surface profile, indicating the roughness of the target surface.

The T-S model is proposed based on the reflection of a rough target surface, and the microstructure of the target surface is represented by the microsurface element theory, which considers that the rough target surface can be viewed as consisting of a series of high and low microsurface elements, and each microsurface element reflection conforms to the law of reflection [16], as shown in Fig. 1.

where n is the normal of each microsurface element, z is the target surface normal, and β is the angle between the incident light and the normal of the microsurface element. The following relationship between the angles is satisfied [8]:

$$\cos(\alpha) = \frac{\cos\theta_i + \cos\theta_r}{2\cos\beta} \tag{3}$$

$$\cos(2\beta) = \cos\theta_i\cos\theta_r + \sin\theta_i\sin\theta_r\cos(\varphi_r - \varphi_i) \tag{4}$$

When the surface of the target object is not an ideal smooth surface, the scattered light incident on the microplane element will be cut off, and the rougher the surface of the object, the greater the probability of occurrence of the masking-masking effect, which will have an effect on the scattering characteristics of the rough object surface, and the mathematically defined equation of the two-way reflection distribution function model of the microplane element with masking function is as follows.

$$f_{BRDF}(\theta_i,\varphi_i,\theta_r,\varphi_r,\lambda) = \frac{1}{2\pi}\frac{1}{4\sigma^2}\frac{1}{\cos^4\alpha}\frac{\exp\left[-\tan^2(\alpha)/2\sigma^2\right]}{\cos\theta_i\cos\theta_r}G(\theta_i,\varphi_i,\theta_r,\varphi_r) \tag{5}$$

where: $G(\theta_{\mathrm{i}},\theta_{\mathrm{r}},\varphi)$represents the object surface shading function, $\theta_i,\theta_r$are the angle between the direction of the incident light, the direction of the reflected light and the normal of the macro object surface, respectively, $\varphi_i,\varphi_r$are the azimuth of the incident light, reflected light, respectively.

The masking function reflects the probability that the two events, absence of masking and shading, occur together [17]. Fig. 2. shows a schematic diagram of the simultaneous occurrence of masking-masking effects.

Based on Fresnel's formula, it is a key step to complete the modeling of the polarization reflection characteristics of the target surface by considering the polarization effect that exists when reflection occurs and establishing the conversion relationship of the polarization states during the reflection of light. According to the electromagnetic field theory, the BRDF is a scalar quantity, and after introducing the vertical component s and the parallel component p, it can represent the polarization characteristics of the vector light and become the polarized BRDF. when calculating the polarization state, the Jones matrix is calculated by the Fresnel formula, and then the correspondence between the Jones matrix and the Muller matrix is used to establish the connection between the reflected light and the incident light [18].

The Mueller matrix is a 4×4 square matrix, After obtaining the Jones matrix, it is coupled with the elements $M_{i,j}$in the Mueller matrix [19], the expression of the Muller matrix is obtained as follows.

$$\boldsymbol{M}\left(\theta_{\mathrm{i}},\theta_{\mathrm{r}},\varphi_{\mathrm{i}},\varphi_{\mathrm{r}}\right) = \begin{bmatrix} M_{00} & M_{10} & M_{20} & M_{30} \\ M_{10} & M_{11} & M_{21} & M_{31} \\ M_{20} & M_{21} & M_{22} & M_{32} \\ M_{30} & M_{31} & M_{23} & M_{33} \end{bmatrix} \tag{6}$$

Taking the T-S model [20] as the base model, introduce (6) into (5) to obtain the first strictly polarized bidirectional reflection

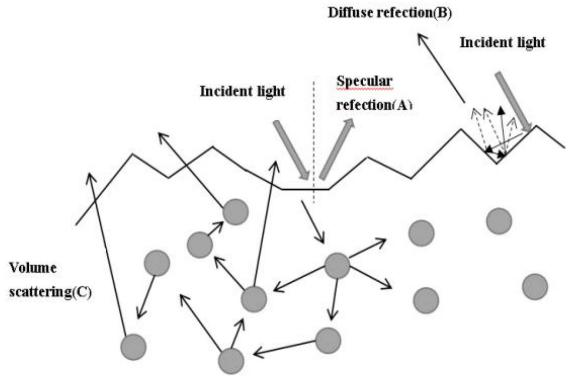

Fig. 3. The target surface's light reflection and shallow layer of the target's light transmission.

distribution function model with the following expression.

$$\boldsymbol{f}_{j,k}\left(\theta_{\mathrm{i}},\varphi_{\mathrm{i}};\theta_{\mathrm{r}},\varphi_{\mathrm{r}}\right)=\frac{1}{2\pi}\frac{1}{4\sigma^{2}}\frac{1}{\cos^{4}\alpha}\cdot\frac{\exp\left(-\tan^{2}\alpha/2\sigma^{2}\right)}{\cos\theta_{\mathrm{i}}\cos\theta_{\mathrm{r}}}\cdot\boldsymbol{M}_{j,k}\left(\theta_{\mathrm{i}},\theta_{\mathrm{r}},\varphi_{\mathrm{i}},\varphi_{\mathrm{r}}\right) \tag{7}$$

Where, j and k are matrix rows and columns, taking values from 0 to 3.

In order to optimize the pBRDF model, it is necessary to analyze the reflection of light on the target surface and the transmission process in the shallow target layer, as shown in Fig. 3.

There are three distinct stages in the process of light reflecting off of non-smooth surfaces. The specular reflection, as seen A in Fig. 3. The diffuse reflection, as seen Bin Fig. 3. The volume scattering, as seen C in Fig. 3.

Treating specular reflection, diffuse reflection and volume scattering separately, the scattering effect of light on the target surface is considered to be in three parts [21]. The expressions for the three-part pBRDF model are given below:

$$f_{pBRDF}=k_{s}\bullet f_{s}+k_{m}\bullet f_{m}+k_{v}\bullet f_{v} \tag{8}$$

Among them, $k_s$is the specular reflection coefficient, k_m is the diffuse reflection coefficient, k_v is the volume scattering coefficient, Distinguished from complex refractive index k; f_s, f_m, f_v are the intensity distribution of specular reflection, diffuse reflection, and volume scattered light, respectively.

Specular reflection section: Introduce the shading factor and Fresnel into the T-S model to obtain the specular component of the scalar BRDF, which is expressed as follows:

$$f_{s}\left(\theta_{i},\theta_{r},\varphi\right)=\frac{P\left(\alpha\right)G\left(\theta_{i},\theta_{r},\varphi\right)F\left(\beta\right)}{4\cos\alpha\cos\left(\theta_{r}\right)\cos\left(\theta_{i}\right)} \tag{9}$$

$F(\beta)$ is the Fresnel reflectivity, whose value is related to the polarization state [22], and is the average of the incident light vertical component reflectivity and incident light parallel component reflectivity. The Fresnel reflectivity in (9) is replaced [23].Then the part of the specular reflection component of the pBRDF model is obtained, and the expression is as follows:

$$f_{j,k}^{s}\left(\theta_{i},\theta_{r},\varphi\right)=\frac{\exp\left(\frac{-\tan^{2}\alpha}{2\sigma^{2}}\right)G\left(\theta_{i},\theta_{r},\varphi\right)M_{j,k}^{s}\left(\theta_{i},\theta_{r},\varphi\right)}{2\pi4\sigma^{2}\cos^{4}\alpha\cos\theta_{i}\cos\theta_{r}} \tag{10}$$

Where, $M_{j,k}^{s}(\theta_i,\theta_r,\varphi)$ is the Mueller matrix of specular reflection. j and k represent the rows and columns of the matrix, and the values are in the range of 0∼3.

In fact, for the specular reflection part, we modeled the shading and shading functions as well as the surface distribution. In the shading and shading function model, the behavior of the light after shading and shading is not described. Therefore a redescription of the shading and shading functions, as well as a description of the higher order effects, is needed to solve the scientific problem.

Assuming that the macroscopically formed phase angle is formed by reflections of order 1, 2 or higher, when there are 2 reflections, the microphase angle is shown in (11).

$$\theta_{2}=\frac{\pi}{2}+\frac{\theta_{1}}{2} \tag{11}$$

where θ_1 is the phase angle and θ_2 is the microphase angle of 2 reflections. Similarly, when the reflections are 3rd, 4th, or higher order reflections, the microphase angles are shown in the following equations, respectively:

$$\theta_{\mathrm{n}}=\frac{(n-1\pi)+\theta_{1}}{\mathrm{n}},\mathrm{n}=2,3,4,\ldots\ldots \tag{12}$$

Extending to the more general case, n can be considered as a non-integer [15], [22]. For higher order specular reflections there are:

$$f_{n}\left(\theta_{i},\theta_{r},\varphi\right)=\frac{\left[G_{n}\left(\theta_{i},\theta_{r},\varphi\right)\right]^{n}\exp[\frac{\tan^{2}(\theta_{n})}{2\sigma^{2}}]M_{j,k}^{s}\left(\theta_{i},\theta_{r},\varphi\right)}{8\pi\sigma^{2}\cos\alpha^{4}(\theta_{n})\cos\left(\theta_{r}\right)\cos\left(\theta_{i}\right)} \tag{13}$$

Taking the polarization of plastic as an example, without considering the surface normal distribution and shadowing and shading functions of the specular micro-element, and considering only the specular reflection at different incidence angles, the pBRDF cases for the 1st order, 2nd order and 0.7+0.3 mixing conditions are shown in Fig. 4.

From Fig. 4, it can be seen from the reflectance that for the 1st reflection, the reflectance increases gently and gradually with the increase of the incident angle, while the 2nd reflection does not have a 0-reflection point and the reflection shape in the upper hemisphere space is bucket-shaped; the polarization of the 1st reflection is spoon-shaped and there is a reflection peak at a position greater than about 90°, and the polarization of the 2nd reflection is spike-shaped and the peak appears in the direction of the 0° incident angle. The reflectance of the 2 reflections is slightly higher than that of the 1 reflection, while the peak polarization of the 2 reflections is lower than that of the 1 reflection. The mixed reflectance and polarization are the combined effect of 2 properties. This hybrid model effectively solves the problem of unclear boundaries when artificially dividing reflections into many different combinations.

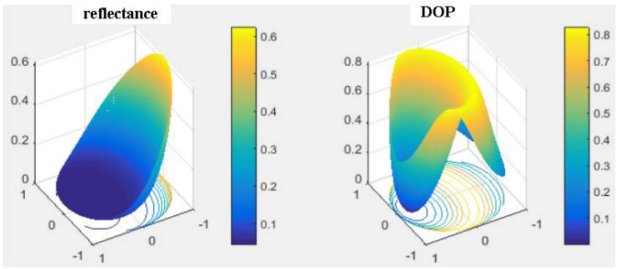

(a). Reflectance and polarization of 1st order reflection.

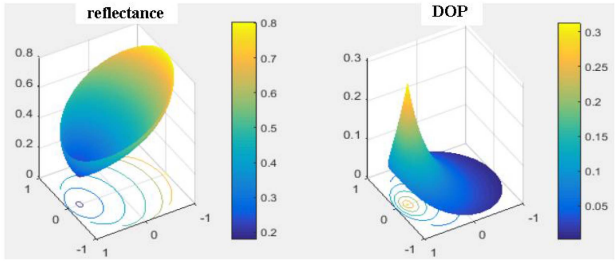

(b). Reflectance and polarization of 2nd order reflection.

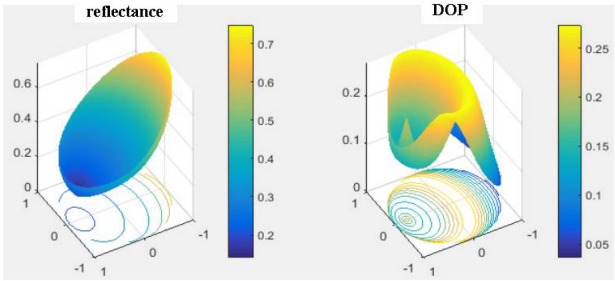

(c) . Reflectance and polarization after mixing.

Fig. 4. Rough surface reflection diagram.

Diffuse reflection section: The magnitude of the angle of incidence has an effect on diffuse reflection [24]. It has its maximum value when the angle of incidence is 0° and decreases as the angle of incidence increases. Therefore, the polarization characteristics of the model are considered in this part, and $f_{j,k}^{m}$ is the diffuse reflection component of the pBRDF model is established, while a Gaussian function distribution is used to describe the variation of the diffuse reflection component [25]. The expressions are given below.

$$f_{j,k}^{m} = \frac{1}{\sqrt{2\pi}\sigma} \exp\left(\frac{-\theta_r^2}{2\sigma^2}\right) M_{j,k}^{m} \tag{14}$$

Among them, $M_{j,k}^{m}$ is the Mueller matrix of diffuse reflection [19], the value of j, k is in the range of 0∼3, if and only if j, $k$are both 0, value is 1,Expressed as $M_{0,0}^{m} = 1$,Otherwise, its value is 0°. Therefore, the diffuse reflection can be considered to be depolarized, and (14) can be simplified to the following expression:

$$f_m = \frac{1}{\sqrt{2\pi}\sigma} \exp\left(\frac{-\theta_r^2}{2\sigma^2}\right) \tag{15}$$

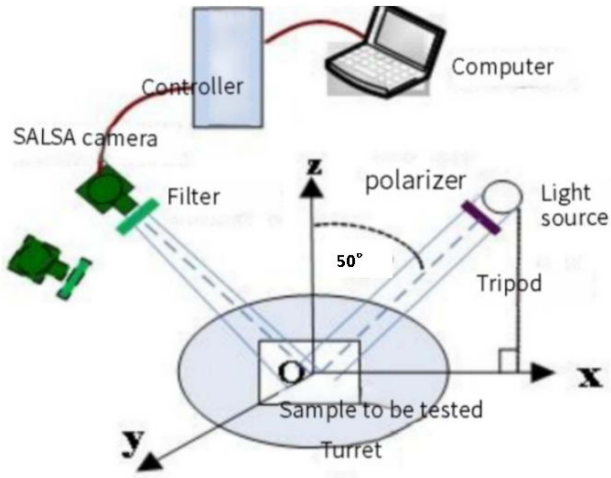

Fig. 5. Principle diagram of polarization characteristics test device.

Volume scattering section: The polarisation state of the incident light changes with the interaction between the photons and the particles inside the material, as the direction of this interaction is random; therefore, the polarisation state of the outgoing light is randomly distributed. However, the photons are equally likely to be distributed in both directions throughout the hemispherical space, so volume scattering can be considered as a result of having the same intensity in all directions. Arrange the bulk scattering part of the pBRDF model $f_{j,k}^{v}$while taking into account the polarisation features in the model. The expressions are given below:

$$f_{j,k}^{v} = 1 \times M_{j,k}^{v} \tag{16}$$

Among them, $M_{j,k}^{v}$ is the Mueller matrix of volume scattering section [19].

Combined with (13), (15) and (16), the degree of polarization under natural light illumination can be calculated, and the expression is as follows:

$$DOP = \sqrt{f_{10}^2 + f_{20}^2}/f_{00} = k_s \cdot f_{s10}/k_s f_{s00} + k_m f_m + k_v f_v = \frac{k_s \times \frac{\exp\left(\frac{-\tan^2\alpha}{2\sigma^2}\right) G(\theta_i,\theta_r,\varphi) M_{10}}{2\pi 4\sigma^2 \cos^4\alpha \cos\theta_i \cos\theta_r}}{k_s \times \frac{\exp\left(\frac{-\tan^2\alpha}{2\sigma^2}\right) G(\theta_i,\theta_r,\varphi) M_{00}}{2\pi 4\sigma^2 \cos^4\alpha \cos\theta_i \cos\theta_r} + k_m \frac{\exp\left(\frac{-\theta_r^2}{2\sigma^2}\right)}{\sqrt{2\pi}\sigma} + k_v} \tag{17}$$

III. Multi-Angle Target Surface Polarization Characteristics Test

An experimental scheme for testing the polarization characteristics of target surfaces indoors is designed and an experimental device is built, which can acquire the polarization images of targets of different materials at different angles. The experimental system of polarization characteristics testing includes three parts: active illumination device, polarization characteristics testing device and information processing device, as shown in Fig. 5.

Fig. 6. SALSA camera appearance diagram.

Fig. 7. physical diagram of the controller.

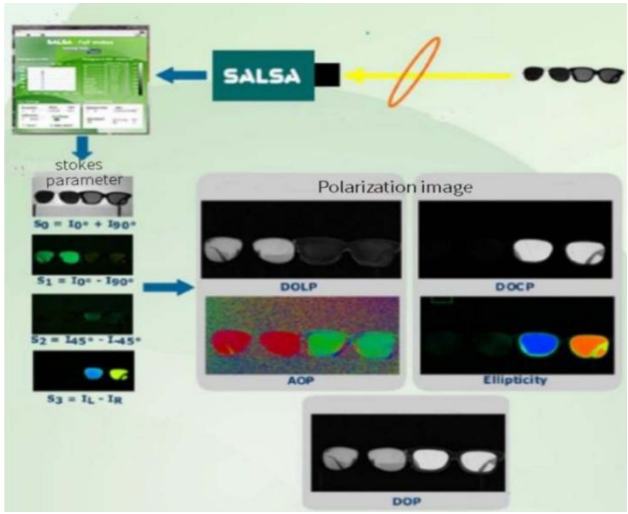

Fig. 8. Information processing schematic.

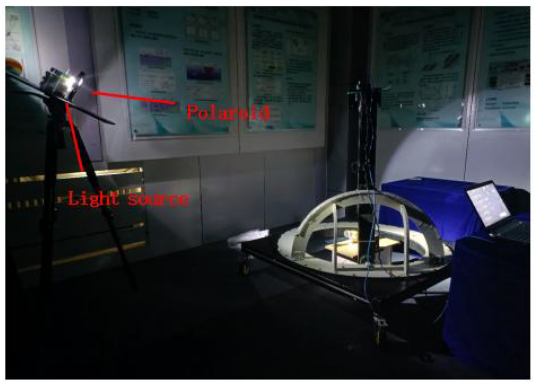

Fig. 9. Data collection scenario diagram.

The polarized light active illumination unit consists of a tripod, a light source and a polarizer. The light source and polarizer are placed together on the tripod and aligned on the same optical axis. The polarization characteristics test device consists of a turntable, a SALSA polarization camera, which controls the angle and distance of detection, and an information processing device consisting of a controller and a computer, which are electrically connected to each other. The controller is also electrically connected to the SALSA polarization camera. The general idea of the experiment is that the light source passes through the polarizer and becomes fully linearly polarized and then hits the target surface, where it is scattered and then the polarization camera receives the information in real time and passes it to the controller, where the data is saved and calculated by the laptop.

The polarization camera is a SALSA polarization camera from Bossa Nova Tech, USA, as shown in Fig. 6. The camera has been factory calibrated with a resolution of 1040*1040 and a frame rate of 12 fps at maximum resolution.

The controller is the medium that connects the information acquisition device and the information processing device, and it has interfaces on the side to the camera and the computer, respectively, as shown in Fig. 7. The controller can synthesize the images acquired by the polarization camera to get the desired polarization image. The schematic diagram of the controller for processing the information is shown in Fig. 8.

First, the equipment was built and installed according to the experimental schematic Fig. 5, and the physical diagram is shown in Fig. 9.

In order to study the differences in polarization characteristics of targets of different materials at different angles, four samples, namely rubber, plastic, plastic and wood board, were selected as test targets in this test. The rubber is natural rubber, isoprene polymer, the plastic is polyethylene, and the plastic cement is PVC. In order to reduce the influence of the sample clock angle on the experiment, we chose square plates with a thickness of 5 mm for several targets.

The polarization image acquisition method was carried out as follows.

Step 1: The measured sample is placed in the center of the rotary table, and the polarizer is rotated to 0 degrees so that the light source gets 0° line polarization light through the polarizer.

Step 2: Rotate the rotating arm on the zenith 2D turntable to the 0° scale, increase the zenith angle by 2° each time, until from 0° to 70° semicircle and the corresponding polarization image acquisition is completed.

Step 3: Rotate the 2D azimuth turntable to expand the azimuth by 2° each time, repeating steps 1 and 2 until the turntable has been rotated from 0° to 360°. The polarization information of the polarized image is then determined.

Step 4: The polarization images taken are synthesized using the controller to obtain the DOP images, and the corresponding

TABLE I
RELATIVE ERRORS OF DOP OF PLASTICS AND PLASTICS CEMENT UNDER THE PROPOSED MODEL AND THE T-S MODEL

	Plastic	decline rate(%)	**Plastic** cement	decline rate(%)
proposed model	6.5918	~	3.2932	~
T-S model	6.6852	1.31	14.4917	77.27

TABLE II
RELATIVE ERRORS OF DOP OF PLANK AND RUBBER CEMENT UNDER THE PROPOSED MODEL AND THE T-S MODEL

	plank	decline rate(%)	rubber	decline rate(%)
proposed model	3.6044	~	2.6843	~
T-S model	5.4648	34.04	3.6044	25.52

polarization degrees are solved and used as the actual measurement data of DOP.

IV. MODEL ACCURACY VERIFICATION AND TARGET POLARIZATION CHARACTERIZATION

In this section, the variation of DOP with the zenith angle was compared for the four materials under the T-S model and the proposed model. As shown in Fig. 10, the top panel shows the T-S model and the bottom panel shows the new model; the red dots are the test data and the solid lines are the simulation data with the parameters substituted into the model.

The relative errors of polarization for different materials under the proposed model and the conventional T-S model are given in Tables I and II.

It can be seen that, compared with the traditional T-S model, the relative error of polarization of plastic is reduced by 1.31%, that of plastic by 77.27%, that of wood by 34.04%, and that of rubber by 25.52% under the improved model. It can be seen that the improved model has higher precision and accuracy.When the detection zenith angle increases to, at this time the detector is in the direction of the specular $\theta_r = \theta_i$reflection of the light source, and most of the light received comes from the specular reflection, so the intensity of polarized light at this time is the highest, and the DOP is also the highest. Therefore, the DOP shows a trend of rising first and then decreasing.

Through simulation and actual measurement data can be obtained, in the detection of the zenith angle of $\theta_r = \theta_i$, that is, in the direction of specular reflection, the polarization of plastic is greater than the polarization of plastic is greater than the polarization of wood board is greater than the polarization of rubber.

This is due to the high proportion of specular reflection generated by the surface of materials with small roughness. The plastic surface is smoother, so the scattering of polarized light becomes smaller, giving the target a higher degree of polarization. Since the target is not a completely smooth surface, it is difficult to achieve 100% DOP.

Plastic and wood panels have a high percentage of diffuse reflections due to their sparse and porous surfaces. Diffuse reflection is depolarizing, resulting in lower polarization of plastic and wood panels than plastic.

Rubber has a small polarization due to its rough surface, which causes polarized light to be scattered many times on its surface. These experimental and simulation results are consistent with conventional knowledge and also verify the accuracy of the model.

V. ARTIFICIAL TARGET CLASSIFICATION BASED ON SCATTERED LIGHT MODEL

Based on the special nature of man-made targets, it is considered that for common man-made objects, scattering can be modeled from the perspective of scattering.

The relationship between incident and scattered light is shown in (18).

$$\begin{vmatrix} E_{//s} \\ E_{\perp s} \end{vmatrix} = \begin{pmatrix} S_2 & 0 \\ 0 & S_1 \end{pmatrix} \cdot \begin{vmatrix} E_{//i} \\ E_{\perp i} \end{vmatrix} \tag{18}$$

The solution of scattered light consists of first solving the vector wave equation in the spherical coordinate system to obtain the solution of the infinite-level representation of the Bessel function, then expanding the incident, scattered and internal fields in the vector spherical covariance function, and finally matching the boundary conditions with the sphere to obtain the infinite-level solution [26]. the expressions of S_1 and S_2 are shown as follows.

$$S_1(\theta) = \sum_{n=1}^{\infty} \frac{2n+1}{n(n+1)} \left[a_n \pi_n(\cos\theta) + b_n \tau_n(\cos\theta)\right] \tag{19}$$

$$S_2(\theta) = \sum_{n=1}^{\infty} \frac{2n+1}{n(n+1)} \left[b_n \pi_n(\cos\theta) + a_n \tau_n(\cos\theta)\right] \tag{20}$$

Where a_n and b_n are the meter coefficients [27], π_n and τ_n are the conjunction Lejeune polynomials [27].

When the particle has a larger refractive index imaginary part or larger diameter, (19), (20) can be directly used for calculation, which can effectively reflect the special nature of the target from the scattering perspective, and can also be used for preliminary classification of the target according to the different results obtained from the calculation of different particle sizes.

The plastic particles selected for the experiment are 10μm in diameter, the wooden board particles are 1μm in diameter, and

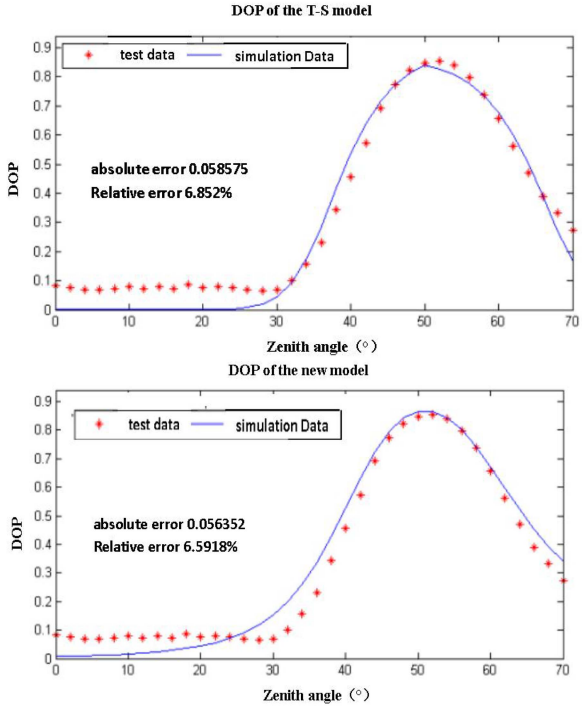

(a). Comparison of DOP of plastics under T-S model and proposed model.

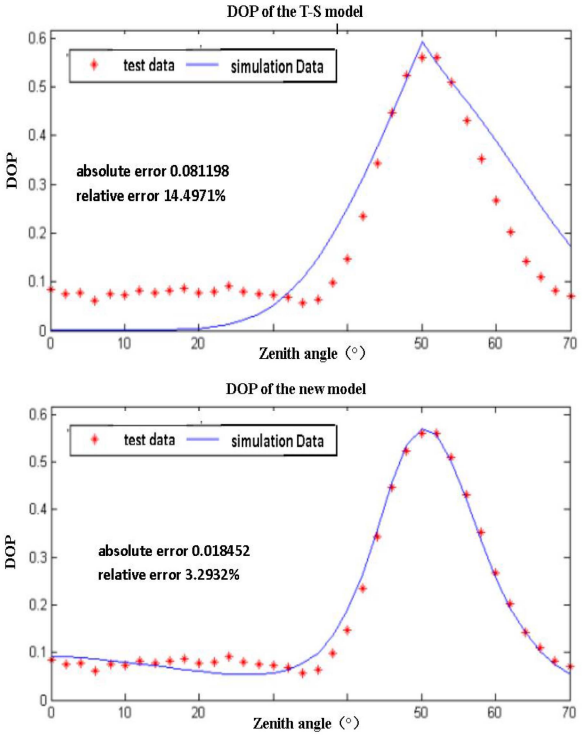

(b). Comparison of DOP of plastics cement under T-S model and proposed model.

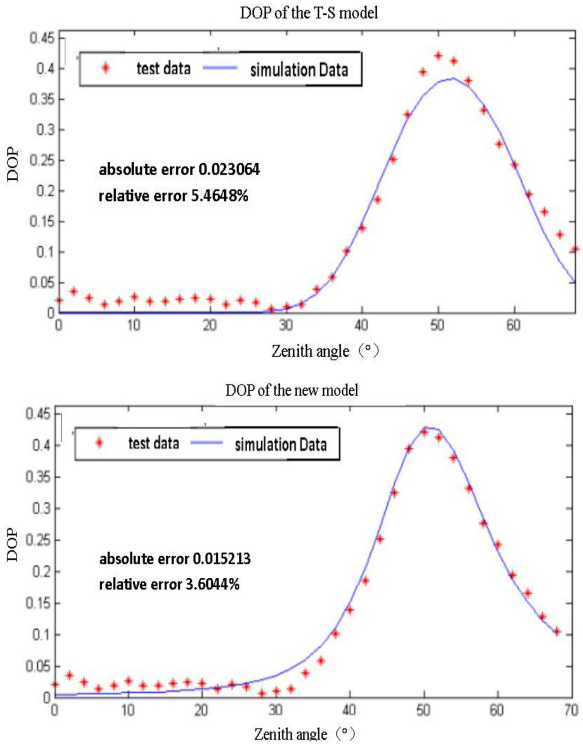

(c). Comparison of DOP of plank under T-S model and proposed model.

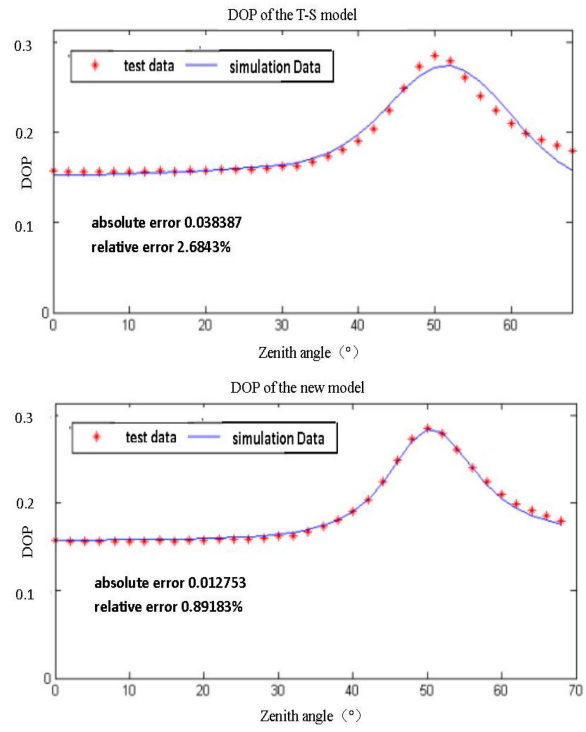

(d). Comparison of DOP of rubber under T-S el and proposed model.

Fig. 10. Comparison of DOP of four materials under T-S model and proposed model.

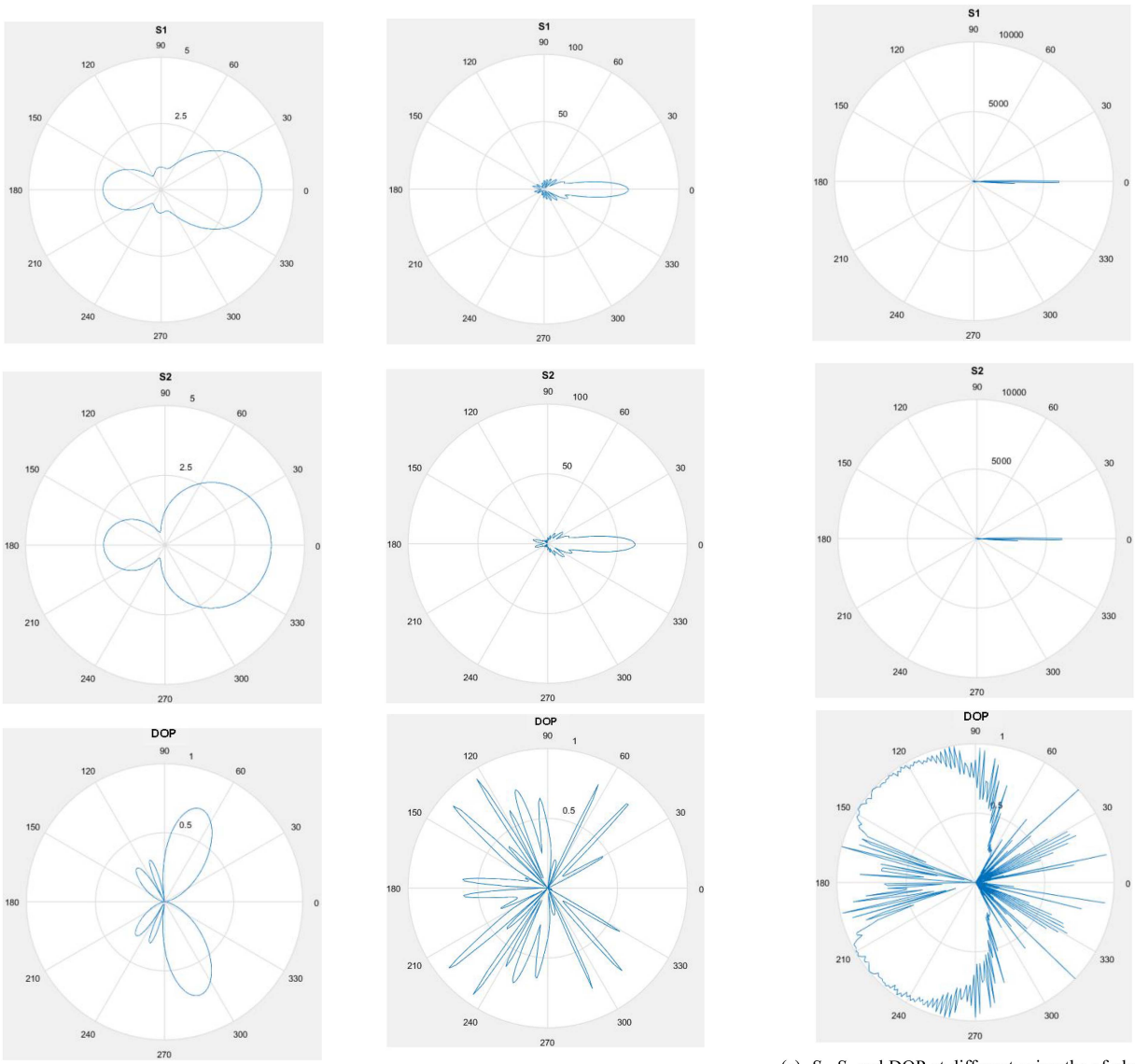

(a). S_1, S_2 and DOP at different azimuths of rubber (particle diameter 0.1 μm).

(b). S_1, S_2 and DOP at different azimuths of plank (particle diameter 1 μm).

(c). S_1, S_2 and DOP at different azimuths of plastic particle diameter 10μm).

Fig. 11. S_1, S_2 and DOP at different azimuths of rubber, plank and plastic.

the rubber particles are 0.1μm in diameter. The main material of plastic cement is PVC, but it contains rubber and pigment particles and other substances, which are mixed chemicals, and the internal particle distribution is not uniform, and the particle diameter is not fixed, so it is not discussed together with the other three materials.

By multiplying and summing the Lejeune expansions of the meter scattering coefficient and the electric field, S_1 and S_2 can be obtained. the sizes of the experimentally selected material particles are 0.1μm, 1μm and 10μm, respectively, then S_1 and S_2 for the rubber particle, the plank and the plastic particle, and the DOP at different azimuths are calculated as shown in Fig. 11.

As can be seen from the figure, there are differences in the intensity and polarization characteristics of the three materials: rubber, wood panel and plastic. As the material changes, the particle diameter becomes larger, the scattering tends to be more forward scattering in terms of intensity; the frequency of intensity and polarization changes with azimuth angle increases; the great value of DOP gradually shifts from forward to backward; and the polarization of plastic is greater than that of wood board than rubber, which is consistent with the proposed model and traditional cognition and verifies the correctness of the model.

According to the special nature of man-made targets, combined with the above experimental conclusions, the scattering angle model can be used to make a preliminary classification of man-made targets.

VI. Conclusion

At different detection angles, the DOP of the sample is different, and the highest DOP of the target is in the mirror reflection direction of the light source. This indicates that the best detection

angle of the polarization detector is the mirror reflection direction. From the analysis of the surface material of the target, when the variables are the same, DOP is plastic, wood plastic cement and rubber in descending order. This indicates that the surface materials of different targets have different polarization characteristics.In recent years, polarization technology is emerging and its application areas are very wide, widely used in atmospheric sounding, military applications, remote sensing detection, earth resource census and medical diagnosis, etc. Its unique advantage of obtaining polarization contrast greatly improves the target identification capability. The polarization information obtained by using the polarization characteristic test is combined with the derived polarization degree expressions. The results show that the established pBRDF model based on the three-component scenario for the target surface can more accurately describe the polarization state of scattered light on the target surface. And the accuracy and precision of the proposed model were verified by comparing with the traditional T-S model.

Using the established scattering model, the relationship between the polarization characteristics and the particle diameter of several different artificial targets is derived. And based on this property, a preliminary classification of different artificial targets can be achieved.

REFERENCES

[1] Q. Fu et al., "Study of sea fog environment polarization transmission characteristics," *Appl. Sci.*, vol. 12, no. 17, pp. 8892, Dec. 2022.

[2] Z. Zhou, X. Liang, and X. Xu, "Spatial polarization characteristics of wide-angle scanning slot phased array," in *Proc. IEEE 12th Int. Symp. Antennas, Propag. EM Theory*, 2018, pp. 1–4.

[3] S. Zhang, J. Zhan, and Q. Fu, "Effects of environment variation of glycerol smoke particles on the persistence of linear and circular polarization," *Opt. Exp.*, vol. 28, no. 14, pp. 20236–20248, 2020.

[4] Q. Fu, F. Zhao, H. Chen, R. Zhu, and Y. Li, "Space object and background polarization models and detect ability analysis," *Appl. Sci.*, vol. 12, Dec. 2022, Art. no. 10714.

[5] D. Yan, G. Qiang, and Y. Fu, "Study on polarization characteristic of asymmetrical AMC structure," in *Proc. IEEE Asia-Pacific Microw. Conf. Proc.*, 2005, Art. no. 3.

[6] Q. Fu et al., "Design and experimental analysis of micropolarization array based on a long-wave infrared optical system," *Appl. Sci.*, vol. 12, Dec. 2022, Art. no. 9802.

[7] Q. Fu et al., "Design and experiment of high-resolution multispectral polarization imaging system," *Appl. Sci.*, vol. 12, Dec. 2022, Art. no. 10712.

[8] H. Shi, Y. Liu, C. He, C. Wang, Y. Li, and Y. Zhang, "Analysis of infrared polarization properties of targets with rough surfaces," *Opt. Laser Technol.*, vol. 151, Oct. 2022, Art. no. 8069.

[9] W. Wang, T. Li, and J. Jiao, "Test method for target full spatial polarization characteristics by BRDF test system," in *Proc. IEEE 12th Int. Symp. Antennas, Propag. EM Theory*, 2018, pp. 1–4.

[10] J. Wen et al., "Forward a small-timescale BRDF/albedo by multisensor combined BRDF inversion model," *IEEE Trans. Geosci. Remote Sens.*, vol. 55, no. 2, pp. 683–697, Feb. 2017.

[11] D. S. Flynn and C. Alexander, "Polarized surface scattering expressed in terms of a bidirectional reflectance distribution function matrix," *J. Opt. Eng.*, vol. 34, pp. 1646–1650, 1995.

[12] T. V. T. Krishna, C. D. Creusere, and D. G. Voelz, "Passive polarimetric imagery-based material classification robust to illumination source position and viewpoint," *IEEE Trans. Image Process.*, vol. 20, no. 1, pp. 288–292, Jan. 2011.

[13] Y. Gu et al., "Polarimetric imaging and retrieval of target polarization characteristics in underwater environment," *J. Appl. Opt.*, vol. 55, pp. 626–637, 2016.

[14] K. E. Torrance and E. M. Sparrow, "Theory for off-specular reflection from roughened surfaces," *J. Opt. Soc. Amer.*, vol. 57, no. 9, pp. 1105–1114, 1967.

[15] J. J. Wang, P. Wang, and F. Y. Wang, "Modified model of polarized bidirectional reflectance distribution function on material surface," *J. Acta Photonica Sinica*, vol. 48, no. 1, 2019, Art. no. 0126001.

[16] F. E. Nicodemus, J. Richmond, and J. Hsia, *Geometrical Considerations and Nomenclature For Reflectance*. Washington, DC, USA: Nat. Bureau of Standards, 1977.

[17] K. P. Gurton and R. Dahmani, "Effect of surface roughness and complex indices of refraction on polarized thermal emission," *J. Appl. Opt.*, vol. 44, no. 26, pp. 5361–5367, 2005.

[18] M. W. Hyde, J. D. Schmidt, and M. J. Havrilla, "A geometrical optics polarimetric bidirectional reflectance distribution function for dielectric and metallic surfaces," *Opt. Exp.*, vol. 17, no. 24, pp. 22138–22153, 2009.

[19] K. Wang and J. P. Zhu, "Degree of polarization based on the three-component pBRDF model for metallic materials," *J. Chin. Phys. B*, vol. 26, no. 2, 2017, Art. no. 024210.

[20] K. E. Torrance and E. M. Sparrow, "Theory for off-specular reflection from roughened surfaces," *J. Opt. Soc. Amer.*, vol. 57, no. 9, pp. 1105–1114, 1967.

[21] K. Wang, J. P. Zhu, and H. Liu, "Expression of the degree of polarization based on the geometrical optics pBRDF model," *J. Opt. Soc. Amer. A Opt. Image Sci. Vis.*, vol. 34, no. 2, pp. 259–263, 2017.

[22] E. Hencht, *Optics*, 4th ed. Boston, MA, USA: Addison Wesley, 1998.

[23] J. P. Zhu, K. Wang, and H. Liu, "Modified model of polarized bidirectional reflectance distribution function for metallic surfaces," *J. Opt. Laser Technol.*, vol. 99, pp. 160–166, 2018.

[24] H. Liu, J. P. Zhu, and K. Wang, "Polarized BRDF for coatings based on three-component assumption," *J. Opt. Commun.*, vol. 384, pp. 118–124, 2017.

[25] M. Yang, W. Xu, and Z. Sun, "Degree of polarization modeling based on modified microfacet pBRDF model for material surface," *J. Opt. Commun.*, vol. 453, pp. 124390, 2019.

[26] K. Liou and J. E. Hansen, "Intensity and polarization for single scattering by polydisperse spheres: A comparison of ray optics and Mie theory," *J. Atmospheric Sci.*, vol. 28, no. 6, pp. 995–1004, 1971.

[27] M. L. Wang, "Parameter identification via shifted Legendre polynomials," *Int. J. Syst. Sci.*, vol. 13, no. 10, pp. 1125–1135, 1982.